ISSN 1063-7710, Acoustical Physics, 2006, Vol. 52, No. 3, pp. 324–330. © Pleiades Publishing, Inc., 2006.
Original Russian Text © O.A. Sapozhnikov, A.E. Ponomarev, M.A. Smagin, 2006, published in Akusticheskiĭ Zhurnal, 2006, Vol. 52, No. 3, pp. 385–392.

Transient Acoustic Holography for Reconstructing the Particle Velocity of the Surface of an Acoustic Transducer

O. A. Sapozhnikov, A. E. Ponomarev, and M. A. Smagin
Faculty of Physics, Moscow State University, Vorob'evy gory, Moscow, 119992 Russia
e-mail: oleg@acs366.phys.msu.ru
Received July 21, 2005

Abstract—A transient acoustic holography method based on the Rayleigh integral and the time-reversal mirror principle is described. The method reconstructs the particle velocity of the surface of an acoustic source from the waveform of the signal measured over a surface lying in front of the source. The possibility of applying the transient holography to studying pulsed sources used in ultrasonic diagnostics is investigated. A rectangular source that produces a short acoustic pulse and has a nonradiating defect on its surface is considered. A numerical simulation is used to demonstrate the possibility of a holographic reconstruction of the source vibrations. The effects of the spatial sampling step and the size of the measurement region on the reconstruction quality are demonstrated.

PACS numbers: 43.60.Sk

DOI: 10.1134/S1063771006030134

INTRODUCTION

The term acoustic holography usually refers to the method of reconstructing an acoustic source from acoustic pressure measured over a surface lying in front of the source. Traditionally, harmonic waves are used. For planar, cylindrical, and spherical sources, the Fourier approach is used, or, in other words, the angular spectrum method [1–4]. The acoustic holography for harmonic signals is in some respects identical to the corresponding version of optical holography, and this similarity made it possible to develop several acoustic holography schemes [5, 6]. However, in acoustics, the following fact is of importance: because the frequency of acoustic signals is lower than that of light waves, the phase of an acoustic wave can be measured directly; i.e., one does not need to use interference with an auxiliary (reference) beam.

The acoustic version of holography also has other advantages, for example, the possibility of performing the measurements at small (compared to the wavelength) distances from the source. In this case, not only the waves that propagate from the source but also the inhomogeneous waves, which exponentially decay with distance from the radiating surface, can be recorded. An appropriate source reconstruction technique achieves a spatial resolution that is much better than the diffraction limit [4]. Another advantage of the acoustic version of holography is that it can be extended to the transient case, for example, to pulse sources, whose spectrum is wide. Formally, the situation is reduced to the case of harmonic waves, because any signal can be represented as a superposition of such waves in the linear approximation. For planar surfaces, transient acoustic holography can therefore be implemented in the framework of Fourier acoustics [3, 7, 8]. An alternative approach [9] relies on the time-reversal mirror principle [10], which requires neither the source surface nor the measurement surface to be planar. This paper describes and improves this version of transient acoustic holography.

One of the important holography applications is the characterization of vibrations of the surfaces of piezoelectric transducers. It is important to be able to measure the normal velocity component at different points of the radiating surface, because it specifies the acoustic sources and, therefore, defines the structure of the acoustic field emitted by the source. The velocity distribution over the surface is usually unknown. It is determined by the transducer design (for example, in the case of multielement arrays) and by the presence of mechanical defects or parasitic modes (for example, of Lamb waves) [11–13]. It should be noted that the familiar laser vibrometry method fails to give correct results when the source is immersed into a liquid, because acoustic interaction produces strong parasitic signals [14]. Acoustic holography is free of this disadvantage. On the other hand, if the distance from the measurement surface to the source is much greater than the wavelength, the holographic reconstruction procedure yields a smoothed surface velocity distribution rather than the true function: irregularities shorter than the wavelength are not reconstructed. This disadvantage does not, however, reduce the importance of the method, because small irregularities emit inhomoge-

neous waves, which do not contribute to the acoustic field produced by the transducer.

An important feature of the experimental investigation of the field produced by a piezoelectric source is that the same ultrasonic field can be produced many times, which allows one to overcome the difficulty inherent in the time-reversal method, namely, the necessity to measure the acoustic pressure simultaneously at a great number of points on the surface of the mirror [10]. Indeed, by exciting the source periodically by the same signal and placing the acoustic sensor at different points of the surface, one can synthesize the time-reversal mirror. The number of measurement points can be as large as several tens of thousands or more. This circumstance provides a high holographic reconstruction quality, which is impossible with the use of the present multielement ultrasonic transducers, where the number of elements can at best be as large as several hundred [10]. The cost of the high quality of the reconstructed hologram is a longer measurement time (up to several hours). Performing this sort of measurements on present automatic facilities usually presents no difficulties.

THEORY

Consider an acoustic transducer with the radiating surface Σ_S (Fig. 1) and the measurement surface Σ_H at a certain distance from the source. The acoustic pressure $p_H(\mathbf{r}', t)$ on the measurement surface is assumed to be known from the experiment. The measured data $p_H(\mathbf{r}', t)$ represent the hologram. Note that both surfaces Σ_S and Σ_H can in general be nonplanar, for example, convex or concave. In particular, this shape is used for ultrasonic sources applied in medical diagnostics and therapy. Due to the latter circumstance, it is impossible to construct a holographic algorithm based on the traditional Fourier acoustics approach. In fact, the angular spectrum method can only be applied to planar and necessarily parallel surfaces Σ_S and Σ_H. We do not limit our analysis to this particular case and consider nonplanar surfaces, although we assume that their curvature is small with respect to the characteristic wave number. This condition is necessary to justify the use of the Rayleigh integral [15, 16].

The problem is to retrieve the acoustic characteristics on the surface of the source from the holographic data $p_H(\mathbf{r}', t)$. This is conceptually possible, because the wave equation can be reversed in time. Imagine that the surface Σ_H is replaced by a time-reversal mirror. Then, the wave reflected from it will propagate backwards and, having reached the source, will reproduce its original characteristics. It was noted [17] that the characteristics will still not be reproduced completely, because, having reached the surface of the source, the reflected wave will not disappear, as would be the case if the time was reversed exactly. It is this circumstance that

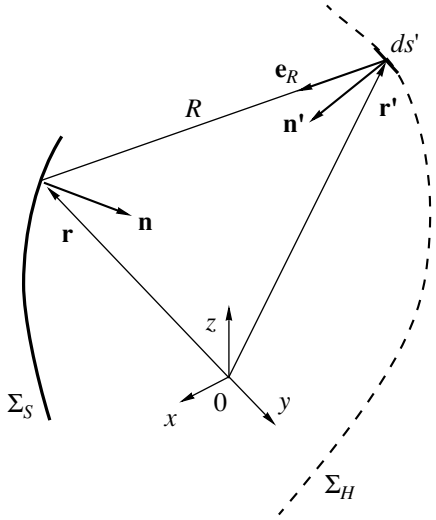

Fig. 1. Arrangement of the surface of the source (Σ_S), the measurement surface (Σ_H), and the corresponding vectors.

imposes the diffraction limit on the reconstruction accuracy. The inhomogeneities on the order of or greater than the wavelength in length must be reconstructed completely.

As follows from the above consideration, the acoustic wave in this holographic procedure is real only when it propagates to the measurement surface Σ_H. At this stage, the experiment ends. The processes of reflection from the time-reversal mirror and of backward propagation are virtual (numerical) [18].

To derive the formulas that describe the process of holographic reconstruction, we first consider the harmonic waves. In this case, the acoustic pressure on the surface Σ_H has the form $p_H(\mathbf{r}', t) = P_H(\mathbf{r}')\exp(-i\omega t) + \text{c.c.}$, and the normal component of the particle velocity on the surface of the source Σ_S is $v(\mathbf{r}, t) = V(\mathbf{r})\exp(-i\omega t) + \text{c.c.}$, where $\omega/2\pi$ is the frequency of the wave and $P_H(\mathbf{r}')$ and $V(\mathbf{r})$ are the complex amplitudes. The velocity amplitude $V(\mathbf{r})$ can be calculated from the pressure amplitude $P_H(\mathbf{r}')$ using the second Rayleigh integral [9]:

$$V(\mathbf{r}) = \int_{\Sigma_H} P_H(\mathbf{r}')K(\mathbf{r}, \mathbf{r}')ds'. \tag{1}$$

The kernel $K(\mathbf{r}, \mathbf{r}')$ is expressed in terms of the normal derivative of the complex conjugate Green's function $G(\mathbf{r}, \mathbf{r}')$ of free space:

$$K(\mathbf{r}, \mathbf{r}') = \frac{2}{i\omega\rho}\frac{\partial^2 G^*(\mathbf{r}, \mathbf{r}')}{\partial\mathbf{n}\partial\mathbf{n}'}, \tag{2}$$

$$G^*(\mathbf{r}, \mathbf{r}') = \frac{e^{-i\frac{\omega}{c}|\mathbf{r}-\mathbf{r}'|}}{4\pi|\mathbf{r}-\mathbf{r}'|}. \tag{3}$$

Here, ρ is the density of the medium, c is the velocity of sound, $\mathbf{n} = \mathbf{n}(\mathbf{r})$ is the unit vector of the outer normal

to the surface of the source at the point of reconstruction $\mathbf{r}$, and $\mathbf{n}' = \mathbf{n}'(\mathbf{r}')$ is the unit normal to the element $ds' \in \Sigma_H$ in the direction toward the source. For example, in the particular case when the surfaces Σ_S and Σ_H are planar and perpendicular to the $0z$ axis, $\partial/\partial\mathbf{n} = \partial/\partial z$ and $\partial/\partial\mathbf{n}' = -\partial/\partial z'$. Let us introduce the following notation: $R = |\mathbf{r} - \mathbf{r}'|$ and $\mathbf{e}_R = (\mathbf{r} - \mathbf{r}')/R$ (see Fig. 1). Then, after taking the derivatives of the Green's function with respect to the normals, expression (2) for the kernel takes the form

$$K(\mathbf{r}, \mathbf{r}') = \frac{e^{-i\frac{\omega}{c}R}}{i2\pi\omega\rho}\left[(\mathbf{n}\cdot\mathbf{n}')\cdot\left(\frac{1}{R^3} + \frac{i\omega}{cR^2}\right)\right.$$
$$\left. - (\mathbf{n}\cdot\mathbf{e}_R)\cdot(\mathbf{n}'\cdot\mathbf{e}_R)\cdot\left(\frac{3}{R^3} + \frac{3i\omega}{cR^2} - \frac{\omega^2}{c^2R}\right)\right]. \quad (4)$$

Calculations and experiments show that the holographic algorithm based on Eqs. (1) and (4) to a high accuracy reconstructs the distribution of the particle velocity over the surface of monochromatic sources, both planar and spherical ones [9, 14, 19].

Now consider transient holography, which reconstructs the velocity $v(\mathbf{r}, t)$ from the measured acoustic pressure $p_H(\mathbf{r}, t)$ in the case of signals of an arbitrary waveform. One of the possible approaches is to change to the spectral density $P_H(\omega, \mathbf{r}) = \int_{-\infty}^{+\infty} p_H(\mathbf{r}, t)e^{i\omega t}dt$ and use Eqs. (1) and (4) to calculate the spectrum $V(\omega, \mathbf{r})$ of the source surface velocity. The velocity is further calculated from $V(\omega, \mathbf{r})$: $v(\mathbf{r}, t) = \frac{1}{2\pi}\int_{-\infty}^{+\infty} V(\omega, \mathbf{r})e^{-i\omega t}d\omega$. Another alternative is to use the time-domain representation. The formula can for example be derived from the spectral representation by integrating with respect to frequency. It is more convenient to write the result for the acceleration $w(\mathbf{r}, t) = \partial v(\mathbf{r}, t)/\partial t$:

$$w(\mathbf{r}, t) = -\frac{1}{2\pi\rho}\int_{\Sigma_H} ds'(\mathbf{n}, \mathbf{n}')\left(\frac{1}{R^3} - \frac{1}{cR^2}\frac{\partial}{\partial t}\right)$$
$$\times p_H\left(\mathbf{r}', t + \frac{R}{c}\right) + \frac{1}{2\pi\rho}\int_{\Sigma_H} ds'(\mathbf{n}, \mathbf{e}_R)(\mathbf{n}', \mathbf{e}_R) \quad (5)$$
$$\times\left[3\left(\frac{1}{R^3} - \frac{1}{cR^2}\frac{\partial}{\partial t}\right) + \frac{1}{c^2R}\frac{\partial^2}{\partial t^2}\right]p_H\left(\mathbf{r}', t + \frac{R}{c}\right).$$

It can be seen that the time dependence of the normal acceleration component can be reconstructed at every point of the surface Σ_S of the source if the waveform of the acoustic signal is known at all points of the measurement surface Σ_H. The contribution of the element ds' is determined by the acoustic pressure and its first and second time derivatives.

NUMERICAL SIMULATION

The practical implementation of transient holography imposes more stringent requirements on the experimental facilities than sinusiodal holography does. In particular, the acoustic sensor must be sufficiently broadband to introduce no distortions into the waveform of the signals being recorded. At each point of the hologram, one should not merely measure the amplitude and phase of the wave, as in stationary holography, but record the entire waveform. Nevertheless, modern instruments and computers are capable of solving this problem. For example, for acoustic waves in the megahertz range applied in medicine and nondestructive testing, miniature wideband PVDF-film-based hydrophones exist. The field can be scanned over the measurement surface by a computer-controlled micropositioning system, and the measured waveforms can be recorded and processed with the help of a personal computer and a dedicated data-acquisition map or a digital oscilloscope [13, 9]. These facilities are available at many acoustic laboratories. To use these possibilities, it is necessary to develop an appropriate algorithm and study it for accuracy and stability with allowance for the constraints imposed by practical measurements. In particular, these constraints include the nonzero sampling interval and the finite size of the measurement window in time and space.

It is convenient to develop the algorithm using numerical simulations. The procedure may be as follows. Specify a reference signal, which is preferred to resemble the one that is used in the physical experiment. Calculate the acoustic field emitted by the transducer from the Rayleigh integral at the points of the surface Σ_H where the acoustic pressure will be measured in the real experiment (the Rayleigh integral is known to very accurately predict the field produced by sources of large wave dimensions [13, 15]). Reconstruct the acceleration on the surface of the transducer by the holographic technique by assuming that the waveforms calculated above are the signals recorded in the hypothetical physical experiment. Finally, compare the resulting space–time distribution with the specified one. The difference between the reference distribution and the reconstructed one is the error of the algorithm.

The Rayleigh integral calculates the acoustic pressure from the normal acceleration $w(\mathbf{r}, t)$ on the surface of the acoustic source:

$$p_H(\mathbf{r}', t) = \frac{\rho}{2\pi}\int_{\Sigma_S}\frac{w(\mathbf{r}, t - R/c)}{R}ds. \quad (6)$$

With a view toward a possible practical application of the method, consider a source like those used in medical diagnostic scanners. The surface of a diagnostic source is often convex (for example, that of the sector scan sensors). In this case, it is also reasonable for the measurement surface to be nonplanar, so that it enve-

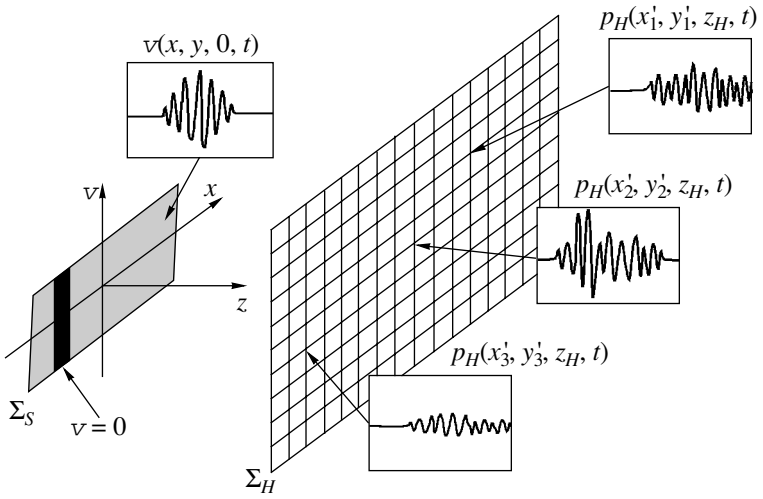

Fig. 2. Geometry of the numerical experiment under study. The rectangular source of acoustic pulses, part of which does not radiate (the black strip), is shown at the left. The holographic data $p_H(\mathbf{r}', t)$ is recorded at the nodes of the rectangular grid. The insets show approximate waveforms at three nodes.

lopes the source and receives the major part of the radiation. However, in this paper, we limit our consideration to a simpler source with a planar radiating surface and we also record the signal at the nodes of a planar grid. Let the radiating surface be a 20×13 mm^2 rectangle radiating short Gaussian pulses (about 2 μs long) at a carrier frequency of 1.55 MHz into the water. Let all points of the source have the same normal velocity component, except for a 2-mm-wide strip where the velocity is zero. This nonradiating strip simulates a damaged region of the sensor (Fig. 2).

The physical experiment (the retrieval of the holographic data) was simulated in terms of Eq. (6). The Rayleigh integral was calculated over a square grid with a step of 0.05 mm on the radiator. The signal waveform was sampled at 33-ns intervals, which are much shorter than the wave period and correspond to 20 samples per period. The calculations were also performed at shorter time and space sampling intervals, which however did not change the results; i.e., the error in calculating the integral in Eq. (6) because of nonzero integration steps was negligible.

Typical fields calculated on the surface of the hologram are shown in Figs. 3a and 3b. They represent the spatial distributions of the peak pressure (a) for a planar unfocused source and (b) for a source focused at a distance of 80 mm. The focusing was achieved by introducing appropriate delays into signals emitted from different points of the surface. In diagnostic sources, this delay is created either with an acoustic lens or by introducing delays into pulses that excite different channels of a multielement transducer. It can be seen that the distribution of the peak pressure over the measurement surface cannot be used to detect and localize the defect on the surface of the ultrasonic sensor in spite of the fact that the distance between the surface and the sensor is rather small (30 mm). As could be expected, the focused source creates a more spatially localized field distribution.

The peak pressure does not carry the full information on the pulsed field. Even if different points of the surface of the source emit pulses of the same waveform, the shape of the acoustic wave at a distance from the source will be different at different points. As an example, Fig. 4 shows the waveform simulated at points *1*, *2*, and *3* shown in Fig. 3a. It can be seen that, at the edge of the measurement region, not only does the peak pressure decrease, but also the signal becomes longer (points *2* and *3*). This is the reason why the time window must be longer than the initial signal; otherwise, the holographic reconstruction error is large.

After the holographic data was calculated at the points of the measurement grid, the initial acceleration distribution over the surface of the source was reconstructed from Eq. (5). The integrals in Eq. (5) were calculated by the rectangle formula, and the time derivatives of the waveform were approximated by central differences. Note that the acoustic pressure in the integrals is taken at times $t + R/c$, which in general causes the discrete instants of the retarded time to shift from the nodes of the initial time grid. Therefore, the pressure should be resampled at each spatial point on the plane of the hologram. To reduce the error, it is reasonable to apply linear interpolation between two adjacent points. Another side of the calculations is the necessity to choose an optimal time window. Because the acoustic signal reaches the measurement region with a substantial delay, it is reasonable to start the recording when the first signal arrives, i.e., within $t_0 = z_H/c$ after the beginning of the radiation. Recording of the signal can be stopped when all possible signals pass through the measurement region.

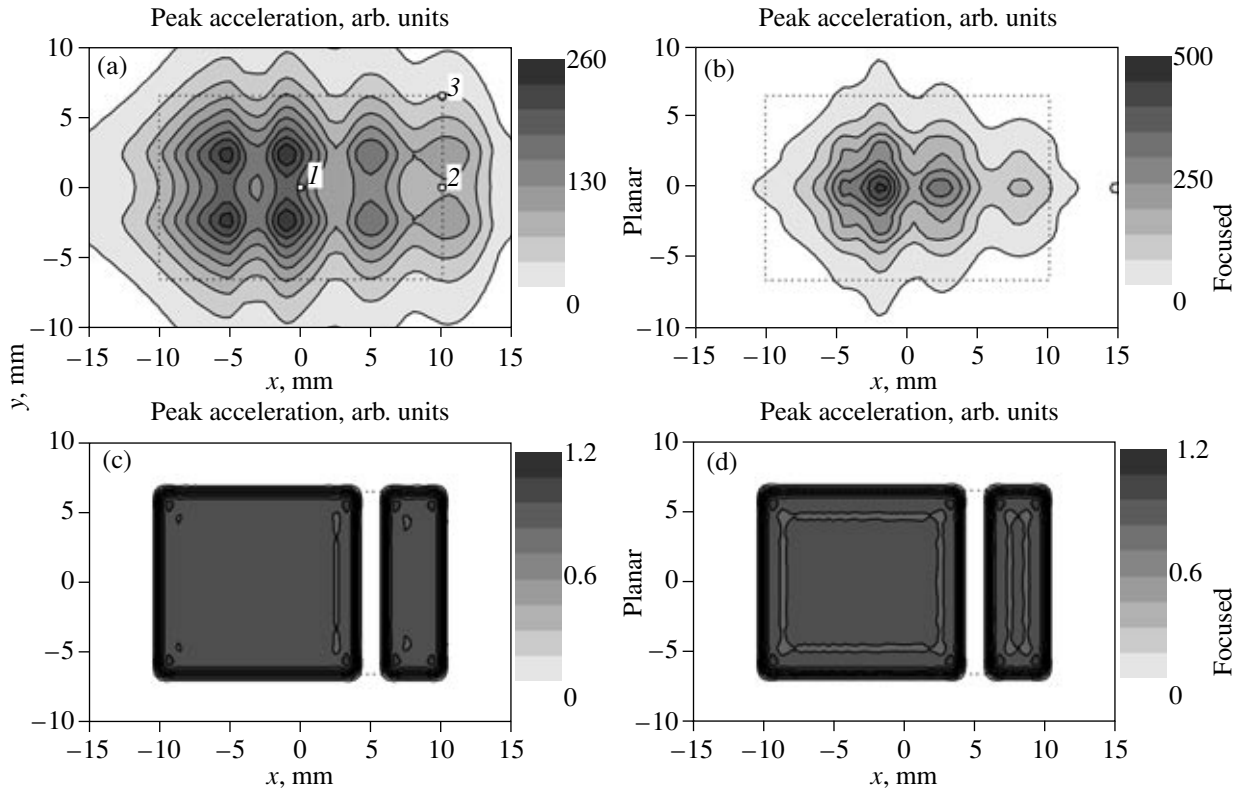

Fig. 3. Two-dimensional gray-scale distributions of the (a, b) peak pressure of the measured pulses and of the (c, d) peak value of the reconstructed acceleration for (a, c) an unfocused planar source and (b, d) a planar source with a focal distance of 80 mm. The distance between the source and the measurement grid is $z_H = 30$ mm; the spatial sampling step is $h = 0.5$ mm. The dotted line is the boundary of the projection of the source.

Figures 3c and 3d show the result of holographic reconstruction of the peak value of normal acceleration on the surface of the source. It can be seen that the distribution of the oscillations on the surface of the source can be reconstructed completely for both the unfocused and focused sources. In particular, one can clearly see the defect (the 2-mm-wide nonradiating strip) and the boundaries of the source. Note again that the distribution of the peak pressure over the surface of the hologram (Figs. 3a and 3b) is insufficient to reveal these features of the surface vibrations of the source.

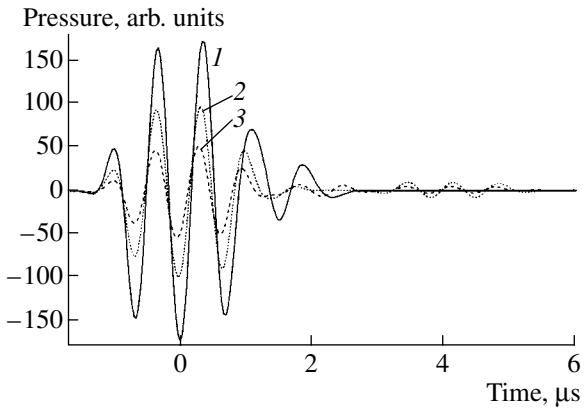

Fig. 4. Acoustic pressure versus time at three measurement points: (0, 0), (10, 0), and (10, 6.5). The respective nodes of the measurement grid are shown in Fig. 3a. The distance between the source and the measurement plane is $z_H = 30$ mm.

The quality of holographic reconstruction in the physical experiment depends on the distance z_H to the source, the spatial sampling steps h_x and h_y, the dimensions x_{max} and y_{max} of the measurement region, and the number of N of measurement points. It is clear that the best reconstruction quality is achieved for $h_x, h_y \longrightarrow 0$ and $x_{max}, y_{max} \longrightarrow \infty$. In practice, an inevitable constraint is that the measurement time is limited; i.e., the number $N = (2x_{max}/h_x)(2y_{max}/h_y)$ of measurement points is finite. At a given number of points, the measurement step can be reduced only by reducing the measurement area. Likewise, the measurement area can be increased only through increasing the measurement step. In each particular case, the optimal parameters can be chosen by numerical simulation. The reconstruction quality can be described in terms of a parameter that characterizes the difference between the reconstructed distribution and the specified one: $\delta w(\mathbf{r}, t) = w_{reconstructed}(\mathbf{r}, t) - w_{exact}(\mathbf{r}, t)$. As the parameter, we can choose, for exam-

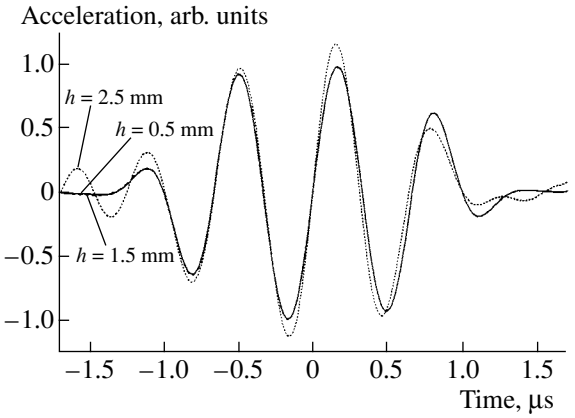

Fig. 5. Time dependence of the acceleration at the center of the source reconstructed at a step of $h = 0.5$, 1.5, and 2.5 mm. The size of the hologram is 120×80 mm^2.

ple, the maximum value of the difference or its rms value on the surface of the source. [19]. In this paper, we do not use these criteria and limit our analysis to qualitative description.

For example, Fig. 5 illustrates the effect of the step size $h = h_x = h_y$ on the quality of reconstruction of the acceleration waveform at the center of the source when the measurement region is sufficiently large (120×80 mm^2). The source in the examples illustrated in Figs. 5 and 6 is unfocused. The results produced by steps of $h = 0.5$ and 1.5 mm are indistinguishable; i.e., a step of about 1 mm is admissible. A further increase in the step produces distortions. It can be seen that, at a relatively large step of $h = 2.5$ mm, the signal waveform is reconstructed with an error; in particular, a spurious precursor appears before the true radiation starts, and the peak pressure slightly increases. The effect of the step of the spatial sampling of the measured field on the quality of reconstruction of the two-dimensional distribution of the peak pressure is illustrated in Fig. 6. It can be seen that, at a step of $h = 1$ mm, the structure of oscillations on the surface of the source is almost perfect (Fig. 6a). The step $h = 1.5$ mm produces certain distortions, but the reconstruction quality is still not bad (Fig. 6b). At the step $h = 2$ mm (Fig. 6c) and, especially, at $h = 2.5$ mm (Fig. 6d), the reconstruction quality cannot be regarded as satisfactory.

Figure 7 illustrates the effect of the size of the measurement region on the reconstructed acceleration. The size of the region decreases from Fig. 7a to Fig. 7d. Calculations show that, for the reconstruction to be adequate, the measurement region must be somewhat larger than the source (Figs. 7a–7c). However, at a small size, the reconstruction can also be satisfactory. In particular, in Fig. 7d, the size of the measurement region (15×10 mm^2) is chosen to be smaller than the size of the source (20×13 mm^2) and the transverse dimension of the acoustic beam (see Fig. 3a). Neverthe-

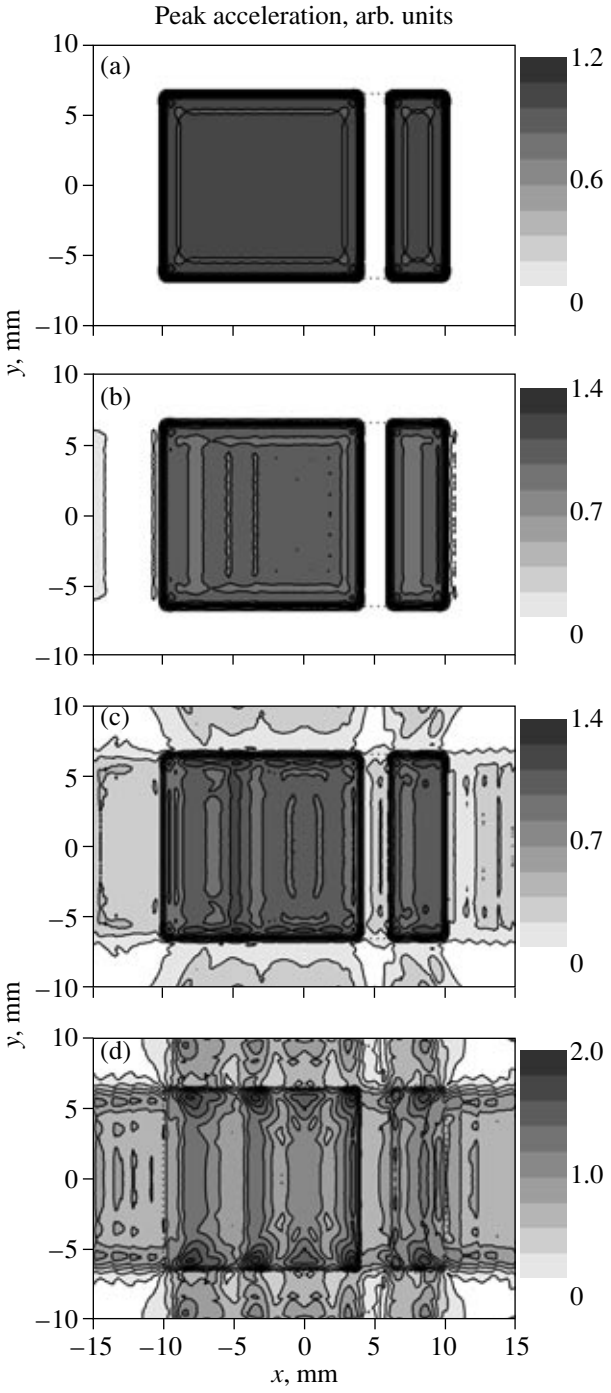

Fig. 6. Two-dimensional distribution of the peak acceleration at a constant hologram size of 120×80 mm^2 and at a step of h = (a) 1.0, (b) 1.5, (c) 2.0, and (d) 2.5 mm. The dotted line is the boundary of the projection of the source.

less, the reconstructed distribution of the peak acceleration can be used to estimate the size of the source and to detect the defect in it. This capability of reconstructing from a fragment of the hologram is similar to the corresponding property of optical holograms. The reconstruction quality is determined by the wave size of

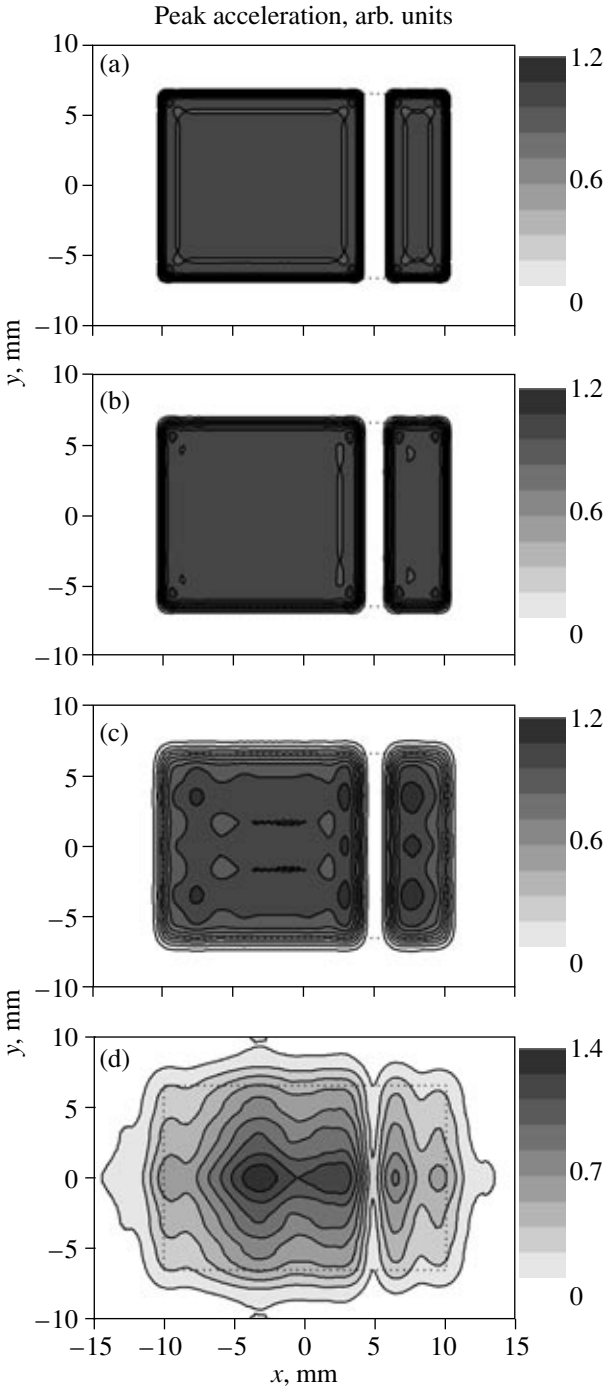

Fig. 7. Two-dimensional distribution of the peak acceleration at a constant the step of $h = 0.5$ mm and a hologram size of (a) 120×80, (b) 60×40, (c) 30×20, and (d) 15×10 mm^2. The dotted line is the boundary of the projection of the source.

the hologram: the greater the hologram in terms of the wavelength, the higher the accuracy of the source reconstruction achieved.

Let us finally note that the algorithm of transient holography described above is a very promising tool for studying the operation of ultrasonic transducers. It can detect rather fine features of the space–time structure of surface vibrations of acoustic sources.

ACKNOWLEDGMENTS

This work was supported by the Russian Foundation for Basic Research, project no. 05-02-16987.

REFERENCES

1. P. R. Stepanishen and K. C. Benjamin, J. Acoust. Soc. Am. **71**, 803 (1982).
2. M. E. Schafer and P. A. Lewin, J. Acoust. Soc. Am. **85**, 2202 (1989).
3. E. G. Williams, *Fourier Acoustics: Sound Radiation and NAH* (Academic, London, 1999).
4. E. G. Williams and J. D. Maynard, Phys. Rev. Lett. **45**, 554 (1980).
5. *Acoustic Holography*, Ed. by V. G. Prokhorov (Sudostroenie, Leningrad, 1975) [in Russian].
6. A. I. Malyarovskiĭ, V. I. Pronyushkin, and Yu. V. Pyl'nov, in *Proceedings of the General Physics Institute, Russian Academy of Sciences. Optoelectronic Data Processing in the Remote Sensing* (Nauka, Moscow, 1990), Vol. 22, pp. 78–106.
7. M. Forbes, S. Letcher, and P. Stepanishen, J. Acoust. Soc. Am. **90**, 2782 (1991).
8. G. T. Clement, R. Liu, S. V. Letcher, and P. R. Stepanishen, J. Acoust. Soc. Am. **104**, 1266 (1998).
9. O. A. Sapozhnikov, Yu. A. Pishchal'nikov, and A. V. Morozov, Akust. Zh. **49**, 416 (2003) [Acoust. Phys. **49**, 354 (2003)].
10. M. Fink, Phys. Today **50**, 34 (1997).
11. B. Delannoy, C. Bruneel, F. Haine, and R. Torguet, J. Appl. Phys. **51**, 3942 (1980).
12. D. Cathignol, O. A. Sapozhnikov, and J. Zhang, J. Acoust. Soc. Am. **101**, 1286 (1997).
13. D. Cathignol, O. A. Sapozhnikov, and Y. Theillere, J. Acoust. Soc. Am. **105**, 2612 (1999).
14. O. A. Sapozhnikov, A. V. Morozov, and D. Cathignol, in *Proceedings of IEEE-UFFC Ultrasonics Symposium, Montreal, 2004* (Montreal, 2004), pp. 161–164.
15. D. Cathignol and O. A. Sapozhnikov, Akust. Zh. **45**, 816 (1999) [Acoust. Phys. **45**, 735 (1999)].
16. O. A. Sapozhnikov and T. V. Sinilo, Akust. Zh. **48**, 813 (2002) [Acoust. Phys. **48**, 720 (2002)].
17. M. Fink, in *Nonlinear Acoustics at the Turn of the Millennium: ISNA15*, Ed. by W. Lauterborn and T. Kurz (Am. Inst. Phys., New York, 2000), pp. 33–44.
18. V. G. Badalyan and E. G. Bazulin, Akust. Zh. **29**, 403 (1983) [Sov. Phys. Acoust. **29**, 238 (1983)].
19. A. V. Morozov, O. A. Sapozhnikov, and Yu. A. Pishchalnikov, Phys. Vibr. **10** (2), 93 (2002).
20. V. A. Khokhlova, A. E. Ponomarev, M. A. Averkiou, and L. A. Kram, Akust. Zh. (2006) (in press).

Translated by A. Khzmalyan